Journal of
Materials Chemistry A

Materials for energy and sustainability

Accepted Manuscript

This article can be cited before page numbers have been issued, to do this please use: J. Gu, X. Zhao, Y. Sun, J. Zhou, C. Sun, X. Wang, Z. Kang and Z. Su, *J. Mater. Chem. A*, 2020, DOI: 10.1039/D0TA04595K.

ROYAL SOCIETY OF CHEMISTRY

rsc.li/materials-a

View Article Online
DOI: 10.1039/D0TA04595K

ARTICLE

Photo-activated process cascaded electrocatalysis for highly efficient CO_2 reduction over core-shell ZIF-8@Co/C

Received 00th January 20xx,
Accepted 00th January 20xx

DOI: 10.1039/x0xx00000x

Jian-Xia Gu,[a] Xue Zhao,[a] Yue Sun,[b] Jie Zhou,[a] Chun-Yi Sun,*[a] Xin-Long Wang,*[a] Zhen-Hui Kang*[b] and Zhong-Min Su[a]

Light irradiation could affect electronic properties of catalysts and the introduction of appropriate light into the electrocatalysts may have a significant impact on the electrocatalytic process, but it has not been fully studied. Herein, we propose a strategy of photo-activated process cascaded electrocatalysis for CO_2 reduction to produce syngas over core-shell ZIF-8@Co/C catalyst. Under light-irradiation, onset potential and overpotential of ZIF-8@Co/C positively shifts by 40 and 200 mV, and syngas production enhances by 5.2-fold at bias potential of -0.9 V vs. RHE. It is noteworthy that the electric energy efficiency promotes by 30%. Deducting syngas generated by electricity, the solar-to-syngas conversion efficiency (Joule to Joule) is up to 5.38% which outperforms reported photoelectrochemical systems. The devices also keep relatively high efficiency in neutral pH aqueous solution. The dedicated experiments and in situ transient photovoltage illuminate the cascaded photo-activation of CO_2 and H^+ in electrocatalysis accounts for the outstanding catalytic performance.

1. Introduction

Excessive utilization of limited fossil fuels accompanied by heavy emission of CO_2 has aggravated global energy crisis and environmental burden.[1-3] The electrochemical reduction of CO_2 to useful chemical stocks or fuels, such as syngas, provides a promising technology to realize a circular carbon-neutral cycle.[4-6] Over the past several years, substantial progress has been made in understanding the transformations of CO_2 since it is kinetically sluggish and intricate reduction process with a high energy barrier. Particularly, the activation of CO_2 molecule which requires a reduction potential of −1.9 V (versus standard hydrogen electrode [SHE]) to reduce linear CO_2 to bent radical anion CO_2^{*-} has the highest energy barrier.[7, 8] Although multi-proton-assisted electron-transfer processes can drive the relatively low activation energy barrier, CO_2 reduction reaction (CO_2RR) remains thermodynamically and kinetically difficult.[9, 10] For example, the thermodynamical equilibrium potential for CO_2 reduction to CO is up to -0.11 V vs. RHE which is quite higher than that of methane, hydrocarbons and alcohols.[11] A substantial amount of additional potential is required to drive CO_2RR. Therefore, a deeper understanding of electrocatalysts-CO_2 activation and the associated kinetics are still necessary, which will lead to more detailed strategies to design CO_2RR catalysts with low overpotential. Note that, light irradiation possibly affects electronic properties of catalysts, such as Fermi level, electron transfer, charge distribution and desorption energy of intermediates, and even influences catalytic pathways.[12] Unfortunately, it is difficult to control these changes induced by light to orientated affect the specific step of catalyst in CO_2 reduction. When a light irradiation process is cascaded directly with the key electrocatalytic step, it may substantially reduce the overpotential and reduce the cost of electric energy. However, there have been few studies investigated the influence of light on CO_2 electroreduction.

Recently, metal-organic frameworks (MOFs) have been considered as great potential catalytic materials in the field of electrocatalysis because of their well-defined composition, large specific surface area, permanent porosity and various catalytic centers .[13, 14] With classical MOF-based material as a catalyst, herein, we report a strategy of photo-activated process cascaded electrocatalysis for highly efficient CO_2RR to produce syngas. Core-shell ZIF-8@Co/C catalyst with hierarchical porous structure is designed based on the following considerations: i) Co/C shell guarantees excellent light absorption and electrical conductivity; ii) mesopores on the shell facilitate the diffusion of substrates; iii) ZIF-8 core acts as CO_2 electrocatalyst for its low cost (0.8$/g) and

[a] National & Local United Engineering Laboratory for Power Batteries, Department of Chemistry, Northeast Normal University, Changchun, Jilin, China. E-mail: suncy009@nenu.edu.cn; wangxl824@nenu.edu.cn.
[b] Jiangsu Key Laboratory for Carbon-Based Functional Materials & Devices, Institute of Functional Nano & Soft Materials (FUNSOM), Soochow University, Suzhou, Jiangsu, China. E-mail: zhkang@suda.edu.cn.
[b] Institute of Advanced Materials, Northeast Normal University, 5268 Renmin Street, Changchun 130024, P.R. China.
Electronic Supplementary Information (ESI) available: Experiment details, characterization and supporting electrochemical and photo-activated electrochemical performances. See DOI: 10.1039/x0xx00000x

View Article Online
DOI: 10.1039/D0TA04595K

convenient synthesis.[15] ZIF-8@Co/C with different shell thicknesses is synthesized by partial pyrolysis of the corresponding ZIF-8@ZIF-67. Without conductive agents, ZIF-8@Co/C exhibits outstanding electrocatalytic performance with Faraday efficiency of syngas (mixture of CO and H_2) generation nearly 100% at -1.2 V vs. RHE. Under light irradiation, the onset potential positively shifts by 40 mV, current density increases by 1.6-fold and syngas production elevates by 5.2-fold at bias potential of -0.9 V vs. RHE together with a decreased overpotential of 200 mV for a similar yield value and a promotion of 30% on electric energy efficiency. Significantly, conversion efficiency (Joule to Joule) of solar energy to syngas (deducting the syngas generated by electricity) is up to 5.38%, which outperforms the reported photoelectrochemical systems. Combined with dedicated electrochemical test and in situ transient photovoalt (TPV), we clearly show that ZIF-8 is more likely to produce CO while Co/C mainly generates H_2 and acts as the main source of photo-induced electrons. The generated photo-induced electrons can orientatedly transfer from Co/C to ZIF-8 to trigger CO_2 activation because of the opposite charge between shell and core of ZIF-8@Co/C catalyst. This photo-activated process cascaded electrocatalysis significantly reduces the overpotential of electrochemical CO_2 reduction (See Scheme 1) and leads to high catalytic performance.

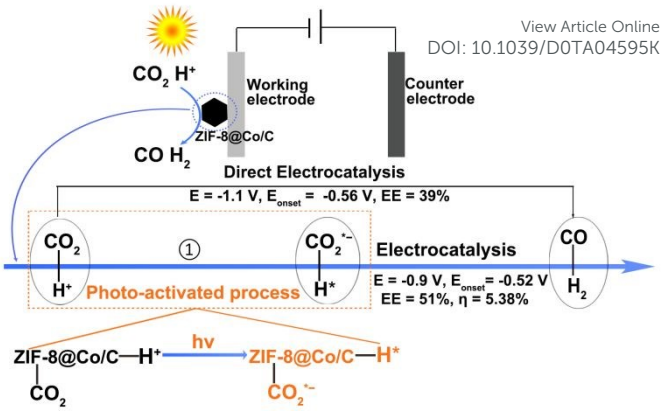

Scheme 1 Diagram of the photo-activated process cascaded electrocatalytic pathway over ZIF-8@Co/C catalyst. (E: optimal applied potential; Eonset: onset potential; EE: electric energy efficiency; η: solar-to-syngas conversion efficiency).

2. Experimental section

Materials

Zinc nitrate hexahydrate ($Zn(NO_3)_2{\cdot}6H_2O$) and 2-methylimidazole (2-MeIm) were purchased from the Shanghai Census Bio-tech Co., Ltd.. Cobalt chloride hexahydrate ($CoCl_2{\cdot}6H_2O$) and methanol were bought from the Fuchen chemical reagent field in the city of Tianjin and Beijing Chemical Works, respectively.

Preparation of the serial of ZIF-8@ZIF-67-x[16] and ZIF-8@Co/C-x (x=1 to 5)

ZIF-8 (80 mg) seed was dispersed in 10 mL of methanol and ultra-sonicated for 30 min. Then, a methanolic solution of $CoCl_2{\cdot}6H_2O$ (177 mg, 3 mL) and a methanolic solution of 2-MeIm (895 mg, 3 mL) were slowly dripped into the above mixture. Subsequently, the mixture was transferred into an autoclave and kept at 100 °C for 12 h. The resulted sample was named as ZIF-8@ZIF-67-4 and was collected by centrifugation after cooling, then washed several times with methanol and dried at 80 °C. The other ZIF-8@ZIF-67-x (x=1, 2, 3, 5, x is defined as the number of samples) with different thicknesses of ZIF-67 shell were prepared by adjusting the amount of $CoCl_2{\cdot}6H_2O$, 2-MeIm and methanol, and the specific amount was shown in the Table S1. The synthetic method is similar to that of ZIF-8@ZIF-67-4.

ZIF-8@Co/C-x (x=1 to 5) was obtained by partial pyrolysis of corresponding ZIF-8@ZIF-67-x (x=1 to 5). The realization of partial pyrolysis strategy is attributed to the difference of pyrolysis temperature of ZIF-8 and ZIF-67.[17] To be specific, the powder of ZIF-8@ZIF-67-x was put into a ceramic boat and transferred into a tube furnace. Then, the powder was heated to 550 °C and kept for 8 min under flowing N_2. When the temperature cooled to room temperature, the ZIF-8@Co/C-x (x=1 to 5) was fabricated. The pyrolysis process of ZIF-8 and ZIF-67 is similar to the above samples.

Electrochemical measurements

The light-irradiation cascaded electrochemical and electrochemical reduction of CO_2 were executed in an H-type cell (Nafion 117 membrane) with a typical three-electrode system. Pt sheet, Ag/AgCl electrode (filled with 3 M KCl) and glassy carbon electrode (GCE) or carbon paper were acted as counter electrode, reference electrode and working electrode, respectively.

The working electrode of light-irradiation cascaded electrochemistry was prepared as following: catalyst (5 mg) was first dispersed in Nafion solution (1.0 mL 0.5%) and ultra-sonicated for 1 h to generate a homogeneous ink. Then, catalyst (20 μL) was dropped onto two sides of carbon paper (0.5*1.0 cm^2) and dried under air atmosphere. K_2SO_4 aqueous solution (0.25 M) was used as the electrolyte according to the reported literature. Before the tests, the electrolyte was purged with CO_2 (or Ar) for 30 min (pH = 4.65, CO_2- saturated K_2SO_4 solution). During measurements, working electrodes were irradiated by a xenon lamp equipped with an AM 1.5 filter. According to the Nernst equation E (RHE) = E (Ag/AgCl) + 0.197 + 0.0591 × pH, all the potentials were calibrated to a reversible hydrogen electrode (RHE). The products of CO_2 electrochemical reduction were detected through gas chromatography (GC) (GC2014, Shimadzu, Japan) equipped with FID and TCD detectors. The process of electrochemical measurement is similar to the light-irradiation cascaded electrochemical test in addition to changing the working electrode and giving no illumination. In this system, GCE (diameter, 3 mm) coated with ZIF-8@Co/C (5 mg/mL, 8 μL) is used as a working electrode. Electrochemical impedance spectroscopy (EIS) measurement was carried out on CHI760 in a frequency range from 100 kHz to 0.01 Hz at a potential of -0.9 V (vs. RHE).

In situ transient photovoltage (TPV) measurements

Under room temperature, the transient photovoltage measurements were carried on films of samples deposited on indium-tin oxide (ITO) glass substrates (1 cm × 1 cm). The films of samples were prepared by dispersing samples (5 mg) into 1.0 ml aqueous (700 μL water, 250 μL ethanol and 50 μL of Nafion solution), then dropped sample aqueous on ITO slides and dried in air. The ITO glass modified with samples as the working electrodes and Pt wire as the counter electrodes were wetted with acetonitrile/H_2O aqueous (v/v=4:0.5). The samples were excited by a laser radiation pulse (wavelength 355 nm, pulse width 5 ns) from a third-harmonic Nd: YAG laser (Polaris II, New Wave Research, Inc.).

3. Results and discussions

Materials characterization

A series of core-shell ZIF-8@ZIF-67-x (x is defined as the number of samples from 1 to 5) with different thicknesses of shell were prepared according to reported methods[16] and through partial pyrolysis of ZIF-8@ZIF-67-x, ZIF-8@Co/C-x were obtained (Fig. 1a). The PXRD (powder X-ray diffraction) pattern of ZIF-8@ZIF-67-x is aligned well with that of bare ZIF-8 or ZIF-67 as the pattern of ZIF-8 and ZIF-67 is similar (Fig. S1a).[16, 18] After pyrolysis, ZIF-8@Co/C-x maintains pristine PXRD pattern of ZIF-8@ZIF-67-x due to intact structure of core ZIF-8 (Inset a of Fig. S1b), but there is a new weak peak at about 44.9° (Fig. S1b) which can be ascribed to cobalt nanoparticles (CoNPs, JCPDS No.15-0806) resulting from the decomposition of ZIF-67 (Inset b of Fig. S1b).[19, 20]

The TEM images of ZIF-8@Co/C-x (x=1 to 5, Fig. 1b and Fig. S3a) retain rhombic dodecahedron morphology of ZIF-8@ZIF-67-x (x=1 to 5, Fig. S2a), except the emergence of rough edge. High-resolution TEM (HRTEM) image of rough edge (Fig. 1c) reveals two types of lattice fringes with d-spacing of 0.21 and 0.36 nm which belong to CoNPs (111) and graphitic carbon (002),[21, 22]respectively, from the decomposed ZIF-67 shell. The elemental mappings (Fig. 1e and Fig. S3c) of Zn and Co in ZIF-8@Co/C-x show they separately distribute in the centre and edge as that in ZIF-8@ZIF-67-x (Fig. S2b), suggesting ZIF-8@Co/C-x maintains core-shell structure.[16, 23] The gradually increased Co content represents an incremental thickness

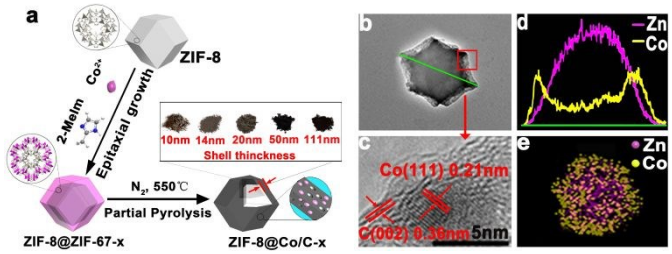

Fig. 1 Preparation and Electron Microscopic Characterization of ZIF-8@ZIF-67 and ZIF-8@Co/C. (a) Schematic illustration of the synthesis process of ZIF-8@ZIF-67-x and ZIF-8@Co/C-x (x=1 to 5). (b) TEM image, (c) HRTEM image, (d) line-scanning spectrum and (e) elemental mapping of ZIF-8@Co/C-4: Zn (purple) and Co (yellow).

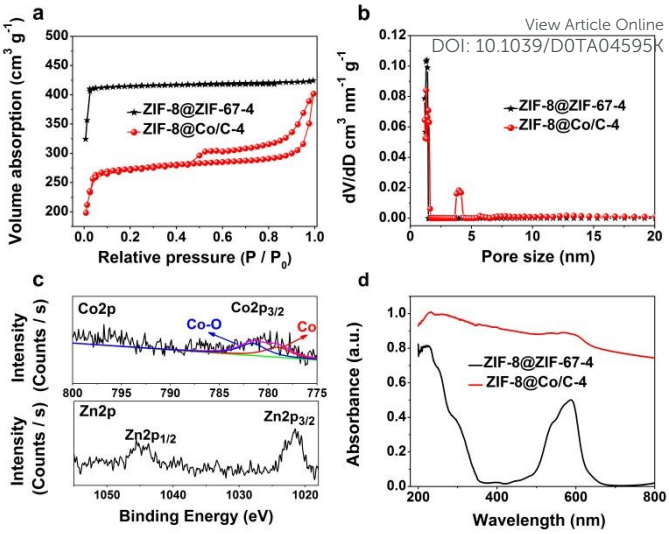

Fig. 2 Structure characterization of ZIF-8@ZIF-67-4 and ZIF-8@Co/C-4. (a) N_2 adsorption–desorption curves of ZIF-8@ZIF-67-4 and ZIF-8@Co/C-4. (b) Pore-size distribution plots of ZIF-8@ZIF-67-4 and ZIF-8@Co/C-4. (c) Co 2p and Zn 2p XPS spectra of ZIF-8@Co/C-4. (d) UV-Vis spectra of ZIF-8@ZIF-67-4 and ZIF-8@Co/C-4.

of Co/C shell. The molar ratios of Co^{2+}/Zn^{2+} are probed by inductively coupled plasma mass spectrometry (ICP-MS) and the thicknesses of Co/C in ZIF-8@Co/C-x are obtained through line scans (Fig. 1d and Fig. S3b), which is depicted in Table S2.

For all ZIF-8@ZIF-67-x (x=1-5), the N_2 adsorption-desorption curves (Fig.2a and Fig. S4) belong to type-I isotherm, which indicates that ZIF-8@ZIF-67-x is a kind of microporous material and the pore size of them is mainly distributed in the range of 1-2 nm (Fig. 2b and Fig. S5). The thickness of the shell has little effect on the N_2 adsorption-desorption as well as pore size distribution of the ZIF-8@ZIF-67-x. In contrast, the N_2 adsorption-desorption curves of ZIF-8@Co/C-x (x=1-5) all belong to type-Ⅳ isotherm with a H3-type hysteresis loop, indicating the existence of abundant mesopores (Fig.2a and Fig. S4)[17, 24, 25]. With the increase of shell thickness in ZIF-8@Co/C-x, the adsorption capacity of nitrogen decreases gradually, which is due to the reduction of specific surface area originating from the transformation of a certain amount of micropores into mesopores after calcination. It is obvious when the shell thickness is lower than 50 nm, the pore size distribution of ZIF-8@Co/C-x (x=1-4) is not affected by the shell thickness, and there are two kinds of pore sizes locating in 1-2 nm and 3-4 nm. Yet, when the thickness of the shell is larger than 110 nm (ZIF-8@Co/C-5), mesopores in the range of 2-3 nm emerges (Fig. 2b and Fig. S5). In a word, ZIF-8@Co/C-x (x=1-5) exhibits hierarchical pore structure, which can facilitate the transport of CO_2 (aq) or CO_2RR relevant species in solution.[26, 27] The specific surface area of ZIF-8@Co/C-x (x=1-5) reduces by 1 %, 8 %, 30 %, 40% and 80 % in comparison with ZIF-8@ZIF-67-x (x=1-5), just shown in Table S3. This decrease is likely due to the increased mesoporous ratio in the ZIF-8@Co/C-x. The CO_2 adsorption capacity of ZIF-8@Co/C-4 is measured to be of ~10.8 cm^3/g (0.44 mmol/g) at room temperature and 1.0 atm (Fig. S6a), suggesting that hierarchical pores offer accessible sites for the

adsorption or capture of CO_2 molecules.[26] X-ray photoelectron spectroscopy (XPS) of ZIF-8@Co/C-4 reveals the predominant existence of C, N, O, Co and Zn element (Fig. S6b). High-resolution XPS spectra at Co 2p and Zn 2p in Fig. 2c suggest that Co^0 and Zn^{2+} species are in the ZIF-8@Co/C-4, which could corroborate the existence of CoNPs[28-30] and ZIF-8[31]. The presence of CoNPs is further witnessed by magnetism of samples in a video (Supporting Material). The diffuse reflectance ultraviolet-visible (UV-Vis) spectrum was used to investigate the optical absorption ability of catalysts. In contrast to the two absorption bands in ZIF-8@ZIF-67-4 (200-350 and 450-650 nm), the UV-Vis spectrum of ZIF-8@Co/C-4 expands the absorption to the whole visible light (400-800 nm) with high intensity (Fig. 2d). Considering ZIF-8 only absorbs the light in the ultraviolet region (Fig. S6c), therefore, the visible-light absorption of ZIF-8@Co/C-x (x=1 to 5, Fig. S6c) mainly originates from Co/C shell. This excellent light absorption ability of ZIF-8@Co/C may provide a prerequisite for the response to light irradiation. The graphitic degree of ZIF-8 and ZIF-8@Co/C-x (x=1 to 5) was investigated by Raman spectroscopy (Fig. S6d). As seen, ZIF-8@Co/C-x (x=1 to 5) shows an obvious peak at about 1500 cm^{-1} and a weak peak near 1300 cm^{-1} which is ascribed to G band and D band of carbon materials, respectively, and indicates a high degree of graphitization in samples.[32] Such structure may lead to high conductivity which conforms to the design requirements for electrocatalysts. But there are no similar peaks in the Raman spectroscopy of ZIF-8, reflecting that disordered carbon and graphite carbon results from pyrolytic ZIF-67.

The electrocatalytic CO_2 reduction

The electrochemical performance of ZIF-8@Co/C was firstly evaluated on the glass carbon electrode (GCE) in K_2SO_4 (0.25M, pH=4.65) aqueous solution following the reported model.[33] As a control, the performance of bare ZIF-8 and Co/C was also studied. Linear sweep voltammetry (LSV) curves at 10 mV s^{-1} from -0.3 to -1.3 V vs. RHE were first tested to evaluate electrocatalytic performance (Fig. 3a and Fig. S7). The current density of these samples in Ar can be ascribed to hydrogen evolution reaction (HER).[34] ZIF-8@Co/C-x (x=1 to 5) and ZIF-8 exhibit a higher current density in CO_2 than that in Ar, while Co/C doesn't present any obvious difference, which implies the active site for CO_2RR in ZIF-8@Co/C may be ZIF-8. Comprehensive product analysis by gas chromatography (GC) reveals that CO and H_2 are the main gas products. And the isotopic experiment was performed by using $^{13}CO_2$ labeling, the ^{13}CO signal (m/z = 29) demonstrates the carbon source of CO indeed derives from the CO_2 used (Fig. S8). Based on the above, we preliminary conclude that ZIF-8 is the main active site of CO generation while Co/C is the centre of H_2 production. In order to further illustrate this conclusion, the yield of CO and H_2 was detected on ZIF-8 and Co/C at -1.2 V vs.RHE. As shown in Fig. S14, H_2 generated by Co/C on GCE is 53.1 times that of ZIF-8, while CO generated by ZIF-8 is 18.7 times that of Co/C, indicating the truth of the above conclusion.

It is found at an optimized applied potential of -1.2 V vs. RHE, the Faradaic efficiency (FE) of CO (Fig. S9a) is negatively correlated

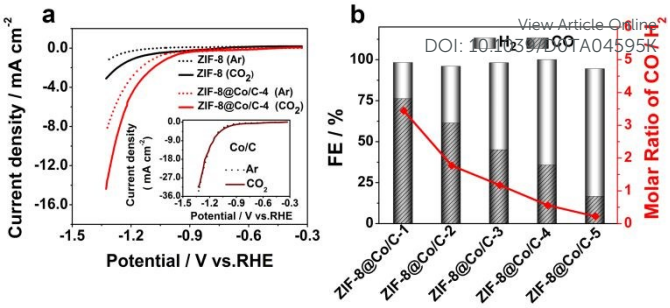

Fig. 3 Electrochemical properties of various catalysts for CO_2RR on GCE. (a) The LSV responses of ZIF-8, ZIF-8@Co/C-4 and Co/C in 0.25 M Ar- and CO_2-saturated K_2SO_4. (b) Faradaic efficiency of CO and H_2 and the corresponding proportions of syngas (CO/H_2) on the ZIF-8@Co/C-x (x=1 to 5) at -1.2 V vs. RHE.

to the thickness of ZIF-8@Co/C shell while the FE of H_2 is just reverse (Fig. S9b). The reason may be that promoted thickness of Co/C shell limits the diffusion of CO_2 to centre ZIF-8, but provides more active sites for H_2 production. These results testify that molar ratios of CO/H_2 are definitely related to composition in catalyst and can be tuned in a large range from 3:1 to 1:5 (Fig. 3b). It is noteworthy that the $FE_{(CO+H2)}$ of these catalysts are all close to 100%. Compared with the performance of reported electrocatalysts (summarized in Table S4) toward syngas generation, the wide range of CO/H_2 ratios achieved on the ZIF-8@Co/C-x is outstanding, and is beneficial to satisfy the demands for various industrial applications, for example, H_2: CO = 0.3−1 is used for syngas fermentation and H_2: CO $\geqslant$ 2 is the important raw materials for methanol synthesis or Fischer-Tropsch reactors.[35-38]

ZIF-8@Co/C-1 is taken as a representation of ZIF-8@Co/C-x for investigating long-term stability. The electrocatalytic stability was evaluated by continuous electrolysis of CO_2 at -1.2 V vs. RHE for 8 h (the analysis of gaseous product by GC every 1.5 h), during which no prominent deactivation of current density and stable FE for CO and H_2 were observed in Fig. S10. Such durability means that ZIF-8@Co/C-x serves as promising electrocatalysts for persistently producing a wide proportion of syngas during CO_2 reduction process.

Light-irradiation cascaded electrochemical CO_2 reduction.

To evaluate the influence of light, Xenon lamp with AM1.5 filter was used. For the inconvenience of light irradiation, the catalyst was dispersed on carbon paper instead of GCE in the light-irradiation cascaded electrocatalysis. First, take ZIF-8@Co/C-4 as an example, LSV curves were tested under dark and light conditions respectively to evaluate the electrocatalytic properties for CO_2 reduction on carbon paper. As a control, the LSV curves of pure ZIF-8 and Co/C were also detected. The current density of ZIF-8@Co/C-4 on carbon paper is all higher in CO_2 than that in Ar both in darkness (Fig.4a) and light irradiation (Fig. S11a). And the trend of LSV curves for ZIF-8 (Fig. S11b) is similar to that of ZIF-8@Co/C-4, suggesting that ZIF-8 and ZIF-8@Co/C-4 have catalytic activity for electrochemical CO_2 reduction. As for Co/C (Fig. S11c), the current density in CO_2 is

View Article Online DOI: 10.1039/D0TA04597C

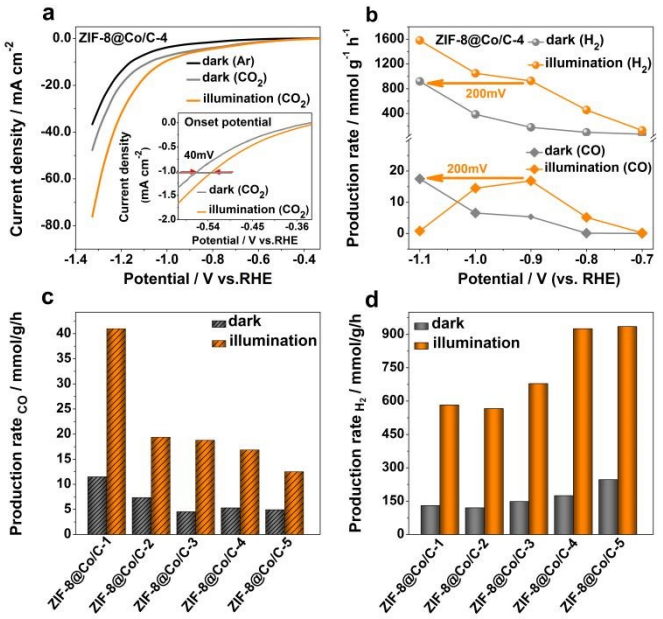

Fig. 4 Light-irradiation cascaded electrochemical performance of CO_2 reduction on the carbon paper. (a) LSV curves of ZIF-8@Co/C-4 in Ar-saturated 0.25 M K_2SO_4 in the dark (black line) and CO_2-saturated 0.25 M K_2SO_4 under illumination (orange line)/dark (gray line). The inset shows the change of onset potential (1 mA cm^{-2}) after illumination in CO_2-saturated 0.25 M K_2SO_4. (b) The curves of production rates for CO and H_2 on ZIF-8@Co/C-4 at different potentials under illumination (orange)/dark (gray). (c, d) The production rates of (c) CO and (d) H_2 on the ZIF-8@Co/C-x (x=1 to 5) in the dark (gray) and illumination (orange) at -0.9 V vs. RHE.

almost identical comparing to that in Ar, meaning the active site for CO_2RR in ZIF-8@Co/C may be ZIF-8. The trend of LSV curves above is all in agreement with that on GCE, indicating the carbon paper doesn't affect the CO_2RR activity of catalysts. With light irradiation, the LSVs of ZIF-8@Co/C-x on carbon paper are obtained and show much enhanced electrochemical activity in contrast to in the dark under similar condition, mainly reflected in the increased current density and the positive shift of onset potential (Fig. 4a and Fig. S12). The current density of ZIF-8@Co/C-x (x=1 to 5) enhances by 1.1 to 1.6-folds at -1.3 V vs. RHE in comparison with that in the dark. The onset potential of ZIF-8@Co/C-x (x=1 to 5) positively shifts by 20 to 40 mV. Among them, ZIF-8@Co/C-4 presents the best performance with a 1.6-fold increase in current intensity and 40 mV shifts of onset potential. The significantly reduced onset potential in the electrocatalysis suggests the introduction of light may be assistant to reduce the energy barrier of CO_2 activation. The best performance of ZIF-8@Co/C-4 may ascribe to the appropriate thickness of shell in light absorption and electron transport.

Based on the above LSVs, the effect of light irradiation on yield of products was also investigated. The potentials were firstly optimized by measuring the yield at different potentials under illumination and -0.9 V vs. RHE was determined to be the best potential for the highest yield of CO (Fig. S13). At this potential, the production rates of CO and H_2 over ZIF-8@Co/C-x (x = 1 to 5) were detected under dark and light irradiation conditions. The production rate of CO (Fig. 4c) declines with the increase of Co/C thickness while that of H_2 (Fig. 4d) rises and the trend is likely to that in the electrocatalysis on GCE (Fig. S9). Besides, H_2 generated by Co/C on carbon paper (CP) is 4.4 times that of ZIF-8, while CO generated by ZIF-8 is 5.1 times that of Co/C (Fig. S14) at -0.9 V vs.RHE, which further indicates that the generation of CO is still mainly on core ZIF-8 while H_2 is on shell and light irradiation doesn't change catalytic center. In comparison with the dark, the yield of syngas on ZIF-8@Co/C-x (x=1 to 5) at -0.9 V vs. RHE enhances by 3.8-5.2 folds under light irradiation (Table S5). The improvement of ZIF-8@Co/C-4 in the amount of syngas exceeds the other four samples and the yield of CO and H_2 reaches 17 and 926 mmol g^{-1} h^{-1}, respectively, under light irradiation. The achievement of similar yield in the dark needs a potential of -1.1 V vs. RHE (Fig. 4b). That is to say, by light irradiation, the overpotential to reach a similar yield value could be reduced by 200 mV. The decreased overpotential further verifies that the cascaded light-irradiation process serves as the role of pre-activation to promote catalytic reactivity. Moreover, the largely increased yield also means that it is possible to improve the electric energy efficiency (EE) of electrochemical process. According to the calculation formula (Supporting Information) of EE, an EE of 51.0% is obtained for ZIF-8@Co/C-4 by light irradiation, which increases by ~30% comparing with that in the dark (39.0%).

Solar energy utilization efficiency in this system is evaluated from the conversion efficiency of Joules of sunlight (in) to Joules of utilizable fuel (out) which is often employed in photocatalysis or photoelectrochemistrysis.[39, 40] The solar-to-syngas (Joules to Joules) energy conversion efficiency of ZIF-8@Co/C-x (x=1 to 5) is calculated as following:[39]

$$\eta = \frac{(n_1 - n_2)_{CO} \times \Delta_c H^0_{CO} + (n_1 - n_2)_{H_2} \times \Delta_c H^0_{H_2}}{P_{solar} \times t}$$

In the equation, n_1 is the molar of CO and H_2 in the light-irradiation cascaded electrochemistry, while n_2 is the molar of CO and H_2 in the electrochemistry. P_{solar} is the input power of the xenon lamp (450 mW cm^{-2}, for 0.25 cm^2 illuminated area). $\Delta_c H_0$ is the standard heat of combustion of H_2 and CO (298.15 K).

The efficiency over ZIF-8@Co/C-x (x=1 to 5) is presented in Table S5. It is found the maximal conversion efficiency is 5.38% over ZIF-8@Co/C-4, which exceeds the reported photoelectrochemical systems (Table S6). At this time, the syngas ratio (H_2/CO) is 54/1 > 50, which can be employed in power generation including gas turbine and fuel cell as well as refinery hydrotreating.[38] ZIF-8@Co/C-4 is taken as a representation of ZIF-8@Co/C-x to study photostability (Fig. S15a). Negligible degradation of the current density and stable molar ratio of H_2/CO are observed on ZIF-8@Co/C-4 catalyst after a continuous test for 8 h at an applied potential of -0.9 V vs. RHE (the analysis of gaseous products by GC every 2 h), suggesting that the as-prepared ZIF-8@Co/C is a durability for electrochemical reduction CO_2 by light irradiation. To further prove the chemical stability of catalyst, XRD of ZIF-8@Co/C-4 was tested after reaction for 8h (Fig. S15b). The main peaks of XRD after reaction for 8h is similar to that before the reaction, revealing its robust chemical stability during the catalysis. After

catalytic reaction for 8h, the XPS of Co2p (Fig. S15c) shows that Co^0 and Co-O species in Co/C shell, which is consistent with Co before reaction and also proves excellent chemical stability of catalyst.

Reproducibility of a catalyst is a key element in electrochemical reduction of CO_2. Thus, take optimal sample ZIF-8@Co/C-4 for example, the catalytic experiments with six batches of the same catalyst were carried out to study the reproducibility under illumination and the yield of products (CO and H_2) at each batch was obtained by gas chromatography. Just shown in Fig. S16, the yield of CO and H_2 is almost identical. And the relative standard deviations (RSDs) are calculated to be 4.9 % for CO and 2.0 % for H_2 from Fig. S16, suggesting the catalyst in this system shows favorable reproducibility for CO_2 electrochemical reduction.

Comparing with high-energy light exposure (with AM 1.5 filter), the production rates of CO and H_2 decrease under visible-light illumination (with 420 nm-cutoff filter), which can be attributed to a component in ZIF-8@Co/C-4 with the wide bandgap led to a limited excitation by visible light. The yield of CO and H_2 on ZIF-8@Co/C-4 still remains 3.2 mmol g^{-1} h^{-1} and 343.5 mmol g^{-1} h^{-1} under visible-light illumination (Fig. S17a), respectively, indicating ZIF-8@Co/C-4 can maintain a satisfying catalytic effect under visible light. It is a favorable signal to make use of sunlight as visible light accounts for ~50% of sunlight. [42] When the light density reduces from 450 to 225 mW cm^{-1} (Fig. S17b), the yield of CO and H_2 just reaches a half indicates there is no photo-induced side-products in the process of reaction. It is found that, in the neutral electrolyte solution (pH=7.12, Fig. S17c), this system is still highly active but relative to the faintly acid solution (pH=4.65), the yield of CO and H_2 descends by 36% (10.7 mmol g^{-1} h^{-1}) and 57% (398.2 mmol g^{-1} h^{-1}). Such a result can be due to the decreased amount of H^+ in the neutral electrolyte solution. The high yield in the neutral electrolyte solution reflects that ZIF-8@Co/C-4 can be applied to electrochemical reduction of CO_2 under a wide range of conditions.

Photo-activated electrocatalytic reduction mechanism

To reveal the rooted reason behind the high reactivity, *in situ* transient photovoalt (TPV) test using different materials as electrodes after adding CO_2 or N_2 was studied firstly. Using bare ZIF-8 as an electrode (Fig. 5a), comparing with the TPV signal in N_2 atmosphere (black curve), the intensity of it in CO_2 atmosphere (red curve) decreases by 61% together with severe trailing, indicating CO_2 may interact with ZIF-8 via multi-step or slow reaction. In contrast, replacing ZIF-8 with Co/C (Fig. 5c), no appreciable difference of TPV signal is found under CO_2 (red curve) and N_2 atmosphere (black curve). These results indicate CO_2 tends to interact with ZIF-8 rather than Co/C. With ZIF-8@Co/C as an electrode (Fig. 5b), the TPV curve in CO_2 atmosphere (red curve) possesses similar slow decay as that of bare ZIF-8 but the intensity undergoes 3-fold enhancement than that of ZIF-8 (red curve, Fig. 5a). These data show that under irradiation, ZIF-8 core in the composite serves as the CO_2 reductive centre, while the Co/C shell mainly takes as the role to absorb light and generates electrons to activate CO_2 and H^+. These inferences basically agree with the conclusions in experiments. When comparing the TPV intensity of

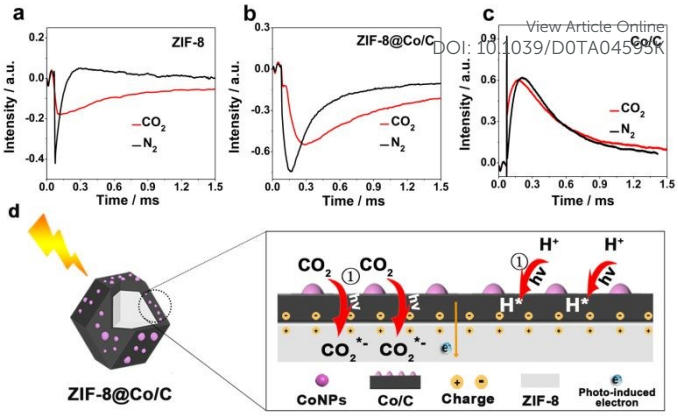

Fig. 5 Mechanism investigation of photo-activated electrocatalytic CO_2 reduction. (a-c) TPV responses of using ZIF-8 (a), ZIF-8@Co/C (b) and Co/C (c) as electrode. (d) The scheme of photo-activated process of CO^2 and H^+ and the process of electron transmission in the catalyst under light irradiation.

ZIF-8@Co/C in N_2 atmosphere (black curve, Fig. 5b) with that of Co/C (black curve, Fig. 5c) in the same condition, we could find 20% enhancement in ZIF-8@Co/C, indicating the core-shell structure facilitate e^-/h^+ charge on the surface of core and shell. The TPV responses for Co/C are positive (red and black curve) (Fig. 5c) while for ZIF-8, they are negative (red and black curve) (Fig. 5a). This nature of opposite charge in core and shell [43, 44] provides an appealing force for the directional flow of photogenerated electrons from Co/C to ZIF-8. This will not only facilitate photo-induced charge separation but accumulate electrons in catalytic sites.

For comprehensively understanding the role of photo-irradiation in electrochemical reduction of CO_2, the electrochemical impedance spectroscopies (EIS) were measured to investigate the effect of light irradiation on the charge transfer resistance (R_{ct}). Nyquist plots of ZIF-8@Co/C-x (x = 1 to 5) were tested in the dark (Fig. S18a) and light irradiation (Fig. S18b). The results illuminate R_{ct} of each catalyst significantly reduces by light stimulation, of particular importance is the R_{ct} of ZIF-8@Co/C-4 which sharply decreases from 103 Ω (in the dark) to 39 Ω (under light irradiation). Such a decrease unambiguously illustrates the influence of the irradiation on relieving the charge transfer resistance and enhancing the efficiency of photo-induced charge separation.

As witnessed by the lowered onset potential and overpotential in the light-irradiation cascaded electrocatalysis, the orientatedly accumulated electrons in ZIF-8 probably participate in the activation of CO_2. Based on the above experimental results and speculative analysis, we conjecture the influence of light irradiation on CO_2 reduction, as shown in Fig. 5d. With the assistance of illumination, photo-induced electrons are generated on Co/C shell and can activate H^+ to form H*, making hydrogen production relatively easy. Benefiting from the force from the opposite charge in core and shell, these electrons also conveniently transfer to ZIF-8 core and trigger the activation of CO_2 adsorbed by sp^2 C atoms of ZIF-8.[33, 45] The above-mentioned process is called photo-activated

process which plays a key role in decreasing energy barrier for CO_2 reduction to prepare syngas.

Compared with the traditional photo-electrocatalysts,[46-48] this photo-activated electrocatalysis integrates the photo-collecting centre and the electrocatalytic site so that the electrons generated by light can directly participate in the electrocatalytic process, rather than converting it into the driving voltage of the external circuit (for traditional photoelectron-catalyst). This change greatly improves the efficiency of photogenerated electron utilization, which may also be the fundamental reason for the high Joule-to-Joule conversion efficiency (5.38% at -0.9 V vs. RHE) of solar energy in our system.

4. Conclusion

In conclusion, we proposed a new photo-activated process cascaded electrocatalysis for efficient CO_2 reduction and synthesized a kind of photo-activated electrocatalyst ZIF-8@Co/C by partial pyrolysis of core-shell porous ZIF-8@ZIF-67. The core-shell and hierarchical porous structure of ZIF-8@Co/C lead to excellent properties in light adsorption and electroconductivity and provides the appealing platform for substrates and intermediates diffusion and adsorption. By adjusting the thickness of shell, syngas within a wide range of CO/H_2 ratio from 3/1 to 1/5 is obtained via electrochemical CO_2 reduction and the FE is nearly 100% at -1.2 V vs. RHE in absence of conductive agents. Motivated by light irradiation, the onset potential and overpotential lower by 40 and 200 mV accompanying with 5.2-fold enhancement in syngas production at a bias potential of -0.9 V vs. RHE. These lead to a 30% promotion on electric energy efficiency. More significantly, high solar-to-syngas (Joule-to-Joule) conversion efficiency is achieved, up to 5.38% which exceeds the value of reported photoelectrochemical systems. The activity of this system could be maintained more than 8 h. The experimental observations and in situ transient photovoltage test illustrate that ZIF-8 is more likely to produce CO while Co/C mainly generates H_2 and acts as the main source of photo-induced electrons. Based on opposite charge between shell and core, the electrons orientatedly transfer from Co/C to ZIF-8 and participate in CO_2 activation which leads to the lowered intrinsic overpotential for CO_2 reduction. This work may open a new avenue to essentially reduce the overpotential of CO_2 electroreduction by introducing the cheap sunlight.

Conflicts of interest

The authors declare no conflict of interest.

Acknowledgments

This work is supported by the National Natural Science Foundation of China (21971032, 21671034, 21471027, 51725204, 21771132, 21471106, 51972216), National MCF Energy R&D Program (2018YFE0306105), the Natural Science Foundation of Jiangsu Province (BK20190041, BK20190828), Guangdong Province Key Area R&D Program (2019B010933001), Collaborative Innovation Center of Suzhou Nano Science & Technology, the Priority Academic Program Development of Jiangsu Higher Education Institutions (PAPD), and the 111 Project.

Notes and references

1 J. Zhao, S. Xue, J. Barber, Y. Zhou, J. Meng and X. Ke, *J. Mater. Chem. A.*, 2020, **8**, 4700-4734.
2 G. Zhao, X. Huang, X. Wang and X. Wang, *J. Mater. Chem. A.*, 2017, **5**, 21625-21649.
3 P. Lamagni, M. Miola, J. Catalano, M. S. Hvid, M. A. H. Mamakhel, M. Christensen, M. R. Madsen, H. S. Jeppesen, X.-M. Hu, K. Daasbjerg, T. Skrydstrup and N. Lock, *Adv. Funct. Mater.*, 2020, **n/a**, 1910408.
4 W. He, I. Liberman, I. Rozenberg, R. Ifraemov and I. Hod, *Angew. Chem. Int. Ed.*, 2020, **n/a**.
5 X. Yang, P. Deng, D. Liu, S. Zhao, D. Li, H. Wu, Y. Ma, B. Y. Xia, M. Li, C. Xiao and S. Ding, *J. Mater. Chem. A.*, 2020, **8**, 2472-2480.
6 X. Wang, D. Wu, C. Dai, C. Xu, P. Sui, R. Feng, Y. Wei, X.-Z. Fu and J.-L. Luo, *J. Mater. Chem. A.*, 2020, **8**, 5105-5114.
7 J. Wu, Y. Huang, W. Ye and Y. Li, *Adv. Sci.*, 2017, **4**, 1700194.
8 Q. Lu and F. Jiao, *Nano Energy.*, 2016, **29**, 439-456.
9 Z. Sun, T. Ma, H. Tao, Q. Fan and B. Han, *Chem*, 2017, **3**, 560-587.
10 Z. Gu, H. Shen, L. Shang, X. Lv, L. Qian and G. Zheng, *Small Methods*, 2018, **2**, 1800121.
11 X. Zhu and Y. Li, *WIREs Comput Mol Sci.*, 2019, **9**, e1416.
12 D. Yang, H. Yu, T. He, S. Zuo, X. Liu, H. Yang, B. Ni, H. Li, L. Gu, D. Wang and X. Wang, *Nat. Commun.*, 2019, **10**, 3844.
13 P. Shao, L. Yi, S. Chen, T. Zhou and J. Zhang, *Journal of Energy Chemistry*, 2020, **40**, 156-170.
14 B.-X. Dong, S.-L. Qian, F.-Y. Bu, Y.-C. Wu, L.-G. Feng, Y.-L. Teng, W.-L. Liu and Z.-W. Li, *ACS Appl. Energy Mater.*, 2018, **1**, 4662-4669.
15 Y. Wang, P. Hou, Z. Wang and P. Kang, *Chemphyschem.*, 2017, **18**, 3142-3147.
16 J. Tang, R. R. Salunkhe, J. Liu, N. L. Torad, M. Imura, S. Furukawa and Y. Yamauchi, *J. Am. Chem. Soc.*, 2015, **137**, 1572-1580.
17 M. Huang, K. Mi, J. Zhang, H. Liu, T. Yu, A. Yuan, Q. Kong and S. Xiong, *J. Mater. Chem. A.*, 2017, **5**, 266-274.
18 Y. Pan, K. Sun, S. Liu, X. Cao, K. Wu, W.-C. Cheong, Z. Chen, Y. Wang, Y. Li, Y. Liu, D. Wang, Q. Peng, C. Chen and Y. Li, *J. Am. Chem. Soc.*, 2018, **140**, 2610-2618.
19 Z. Hu, Z. Zhang, Z. Li, M. Dou and F. Wang, *ACS Appl. Mater. Interfaces*, 2017, **9**, 16109-16116.
20 Y. J. Sa, S. O. Park, G. Y. Jung, T. J. Shin, H. Y. Jeong, S. K. Kwak and S. H. Joo, *ACS Catal.*, 2019, **9**, 83-97.
21 L. Wei, L. Qiu, Y. Liu, J. Zhang, D. Yuan and L. Wang, *ACS Sustainable Chem. Eng.*, 2019, **7**, 14180-14188.
22 T. Yang, K. Li, L. Pu, Z. Liu, B. Ge, Y. Pan and Y. Liu, *Biosens. Bioelectron.*, 2016, **86**, 129-134.
23 J. Zhang, Y. Wang, K. Xiao, S. Cheng, T. Zhang, G. Qian, Q. Zhang and Y. Feng, *New J. Chem.*, 2018, **42**, 6719-6726.
24 Y.-N. Gong, L. Jiao, Y. Qian, C.-Y. Pan, L. Zheng, X. Cai, B. Liu, S.-

View Article Online
DOI: 10.1039/D0TA04595K

H. Yu and H.-L. Jiang, *Angew. Chem. Int. Ed.*, 2020, **59**, 2705-2709.
25 J. Liu, X. Bo, M. Zhou and L. Guo, *Mikrochim. Acta.*, 2019, **186**, 639.
26 W. Ni, Y. Xue, X. Zang, C. Li, H. Wang, Z. Yang and Y.-M. Yan, *ACS Nano.*, 2020, **14**, 2014-2023.
27 J. Gu, X. Yin, X. Bo and L. Guo, *ChemElectroChem*, 2018, **5**, 2893-2901.
28 H. Yu, B. Zhang, F. Sun, G. Jiang, N. Zheng, C. Xu and Y. Li, *Appl. Surf. Sci.*, 2018, **450**, 364-371.
29 Z. Wang, Y. Lu, Y. Yan, T. Y. P. Larissa, X. Zhang, D. Wuu, H. Zhang, Y. Yang and X. Wang, *Nano Energy.*, 2016, **30**, 368-378.
30 D. Lyu, Y. Du, S. Huang, B. Y. Mollamahale, X. Zhang, S. W. Hasan, F. Yu, S. Wang, Z. Q. Tian and P. K. Shen, *ACS Appl. Mater. Interfaces*, 2019, **11**, 39809-39819.
31 M. Zhang, Q. Shang, Y. Wan, Q. Cheng, G. Liao and Z. Pan, *Appl. Catal. B Environ.*, 2019, **241**, 149-158.
32 L. Wang, Z. Wang, L. Xie, L. Zhu and X. Cao, *ACS Appl. Mater. Interfaces*, 2019, **11**, 16619-16628.
33 X. Jiang, H. Li, J. Xiao, D. Gao, R. Si, F. Yang, Y. Li, G. Wang and X. Bao, *Nano Energy*, 2018, **52**, 345-350.
34 H.-J. Zhu, M. Lu, Y.-R. Wang, S.-J. Yao, M. Zhang, Y.-H. Kan, J. Liu, Y. Chen, S.-L. Li and Y.-Q. Lan, *Nat Commun.*, 2020, **11**, 497.
35 W. Sheng, S. Kattel, S. Yao, B. Yan, Z. Liang, C. J. Hawxhurst, Q. Wu and J. G. Chen, *Energy Environ. Sci.*, 2017, **10**, 1180-1185.
36 B. Qin, Y. Li, H. Fu, H. Wang, S. Chen, Z. Liu and F. Peng, *ACS Appl. Mater. Interfaces*, 2018, **10**, 20530-20539.
37 M. B. Ross, C. T. Dinh, Y. Li, D. Kim, P. De Luna, E. H. Sargent and P. Yang, *J. Am. Chem. Soc.*, 2017, **139**, 9359-9363.
38 S. Hernández, M. Amin Farkhondehfal, F. Sastre, M. Makkee, G. Saracco and N. Russo, *Green Chem.*, 2017, **19**, 2326-2346.
39 S. Sorcar, Y. Hwang, J. Lee, H. Kim, K. M. Grimes, C. A. Grimes, J.-W. Jung, C.-H. Cho, T. Majima, M. R. Hoffmann and S.-I. In, *Energy Environ. Sci.*, 2019, **12**, 2685-2696.
40 Y. Wang, J. Liu, Y. Wang, Y. Wang and G. Zheng, *Nat. Commun.*, 2018, **9**, 5003.
41 C. Kim, S. Hyeon, J. Lee, W. D. Kim, D. C. Lee, J. Kim and H. Lee, *Nat. Commun.*, 2018, **9**, 3027.
42 D. Li, S.-H. Yu and H.-L. Jiang, *Adv. Mater.*, 2018, **30**, 1707377.
43 Y. Lu, Y. Lin, T. Xie, S. Shi, H. Fan and D. Wang, *Nanoscale.*, 2012, **4**, 6393-6400.
44 Y. Lu, Y. Lin, D. Wang, L. Wang, T. Xie and T. Jiang, *Nano Res.*, 2011, **4**, 1144-1152.
45 S. Dou, J. Song, S. Xi, Y. Du, J. Wang, Z. F. Huang, Z. J. Xu and X. Wang, *Angew. Chem. Int. Ed.*, 2019, **58**, 4041-4045.
46 N. Zhang, R. Long, C. Gao and Y. Xiong, *Sci China Mater.*, 2018, **61**, 771-805.
47 A. U. Pawar, C. W. Kim, M.-T. Nguyen-Le and Y. S. Kang, *ACS Sustainable Chem. Eng.*, 2019, **7**, 7431-7455.
48 S. Chu, S. Fan, Y. Wang, D. Rossouw, Y. Wang, G. A. Botton and Z. Mi, *Angew. Chem. Int. Ed.*, 2016, **55**, 14262-14266.

View Article Online
DOI: 10.1039/D0TA04595K

Graphical abstract

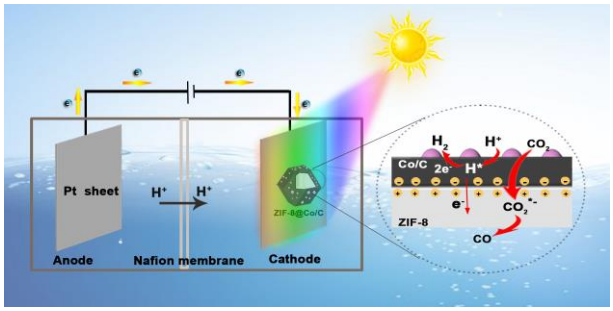

A photo-activated process is cascaded to electrocatalytic pathway for reducing CO_2 to prepare syngas over core-shell ZIF-8@Co/C, exhibiting excellent electrochemical performance and achieving high Joule-to-Joule conversion efficiency of 5.38%.